

SUPPORTING INFORMATION

Topochemical Modulations from 1D Iron Fluoride Precursor to 3D Frameworks

Arindam Ghosh^a, Dereje Bekele Tekliye^d, Emily E. Foley^e, Varimalla Raghavendra Reddy^f, Raphaële J. Clément^e, Gopalakrishnan Sai Gautam^d, Premkumar Senguttuvan^{a,b,c,}*

^aNew Chemistry Unit, ^bInternational Centre for Materials Science and ^cSchool of Advanced Materials, Jawaharlal Nehru Centre for Advanced Scientific Research, Jakkur, Bangalore-560064, India.

^dDepartment of Materials Engineering, Indian Institute of Science, Bengaluru, 560012, Karnataka, India.

^eMaterials Department, Materials Research Laboratory, University of California Santa Barbara, Santa Barbara, California 93106, United States.

^fUGC-DAE Consortium for Scientific Research, University Campus, Khandwa Road, Indore 452001, India.

Author information

*Corresponding Author. Jawaharlal Nehru Centre for Advanced Scientific Research, Jakkur, Bangalore-560064, Karnataka, India

*E-mail: prem@jncasr.ac.in,

ORCID

Arindam Ghosh: 0000-0001-9014-7345

Emily E. Foley: 0000-0003-2173-7899

Raphaële J. Clément: 0000-0002-3611-1162

Gopalakrishnan Sai Gautam: 0000-0002-1303-0976

Premkumar Senguttuvan: 0000-0001-8465-5896

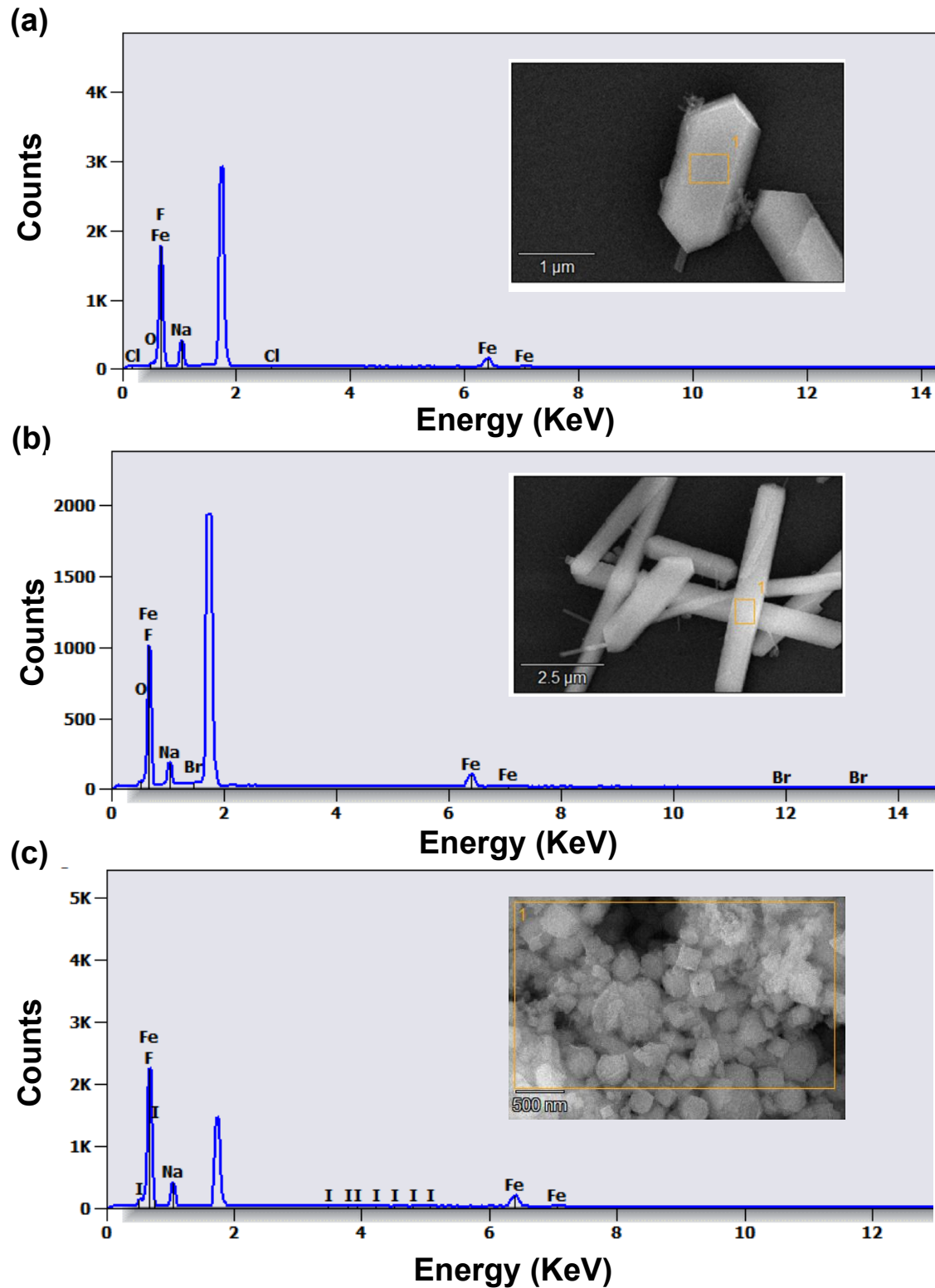


Figure S1: EDX spectrum and the SEM images of the obtained product after reacting fluoride precursor with (a) NaCl, (b) NaBr, and (c) NaI.

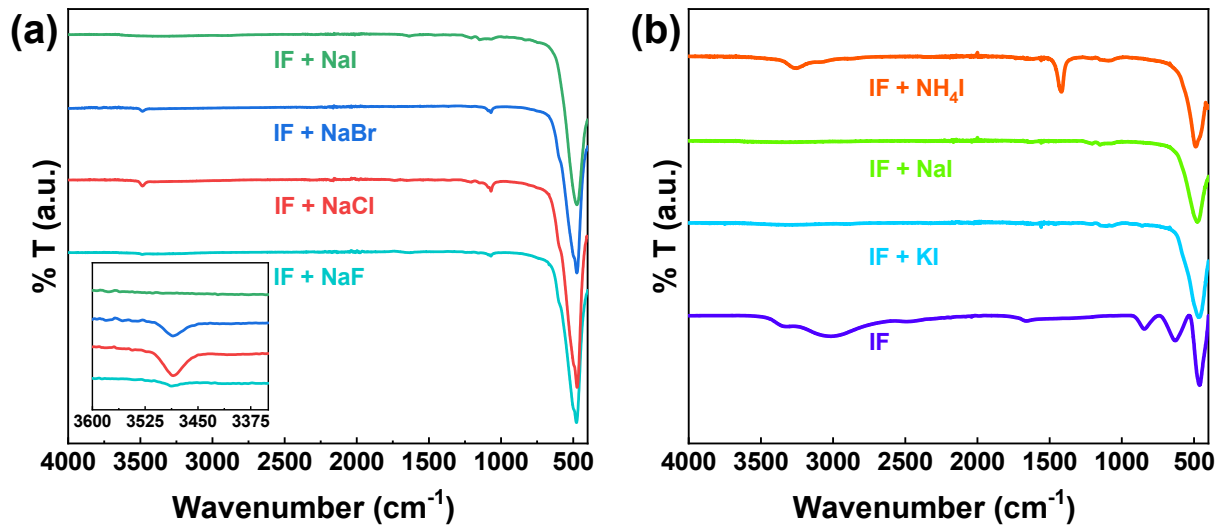


Figure S2: (a) FTIR spectra collected on the products of reactions between IF and NaF/NaCl/NaBr/NaI (Inset: magnified section around the O-H stretching frequency region). (b) Comparison between IR patterns of IF precursor and the final products from the reactions of AI:IF = 1:1 ($\text{A}^+ = \text{Na}^+, \text{K}^+, \text{and } \text{NH}_4^+$).

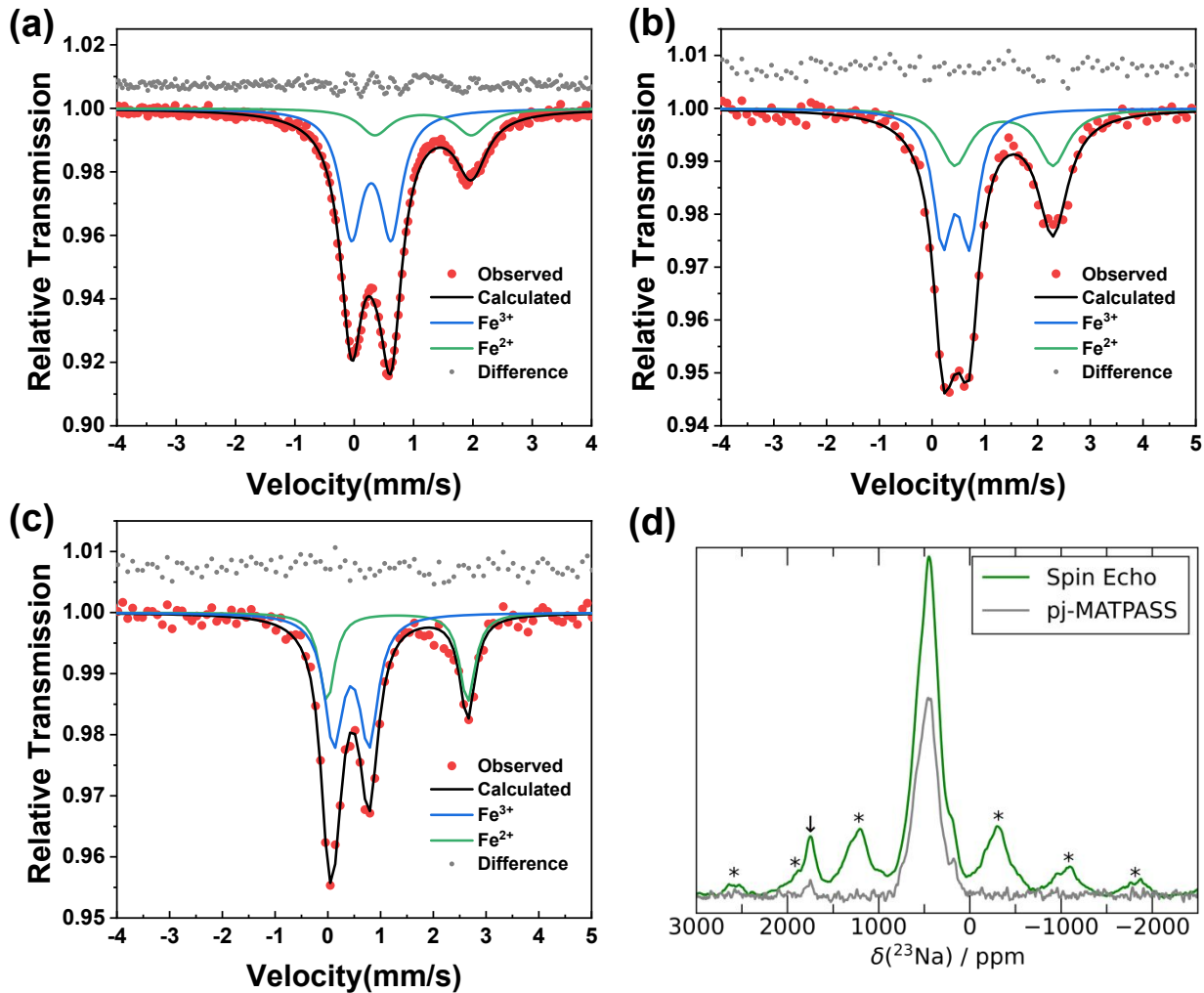


Figure S3: ^{57}Fe -Mössbauer spectra of (a) weberite (b) TTB and (c) pyrochlore phases. (d) ^{23}Na solid-state NMR spin echo and pj-MATPASS spectra¹ collected on weberite- $\text{Na}_2\text{Fe}_2\text{F}_7$. While the spin echo spectrum exhibits sidebands (denoted with asterisks) due to fast spinning of the sample at the magic angle (MAS) during data acquisition, the pj-MATPASS spectrum only contains isotropic resonances and allows us to identify the resonant frequency of each distinct Na environment in the sample. The arrow indicates the resonance corresponding to amorphous Na_3FeF_6 .

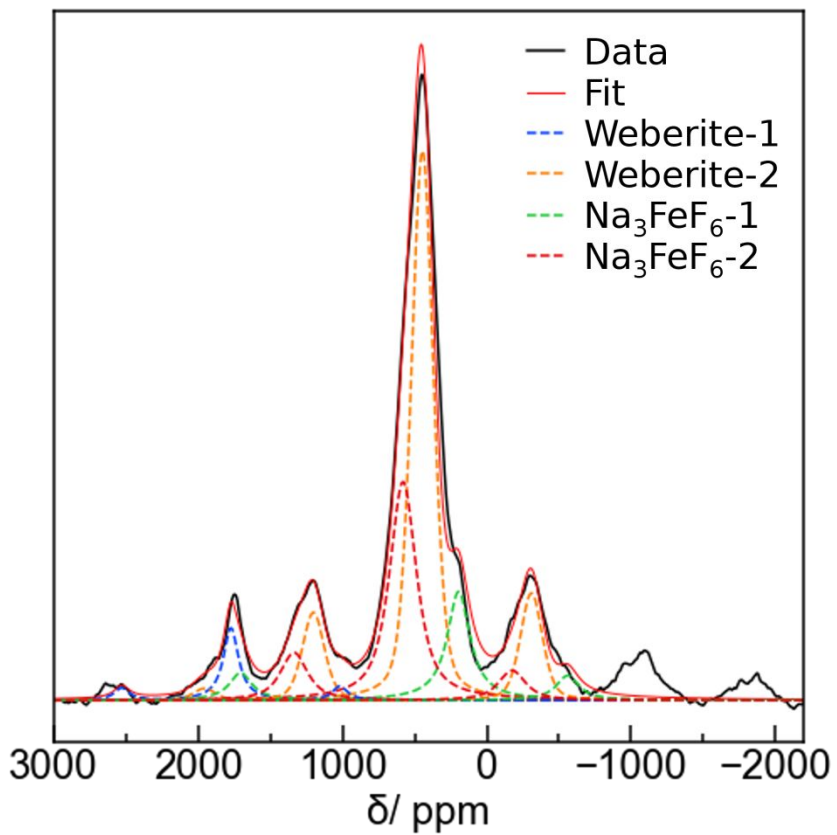


Figure S4: Quantitative ^{23}Na NMR spin echo spectrum for $\text{Na}_2\text{Fe}_2\text{F}_7$ (duplicated from Figure S2d) and its corresponding fit of individual resonances. The chemical shifts for the signals corresponding to Na_3FeF_6 ($\delta = 350$ and 1750 ppm) and their intensity ratio (2:1) were fixed to agree with that previously reported for Na_3FeF_6 . Spinning sidebands are indicated by asterisks (*) and the arrow indicates the isolated resonance corresponding to amorphous Na_3FeF_6 identified in the pj-MATPASS spectrum in Figure S2d.

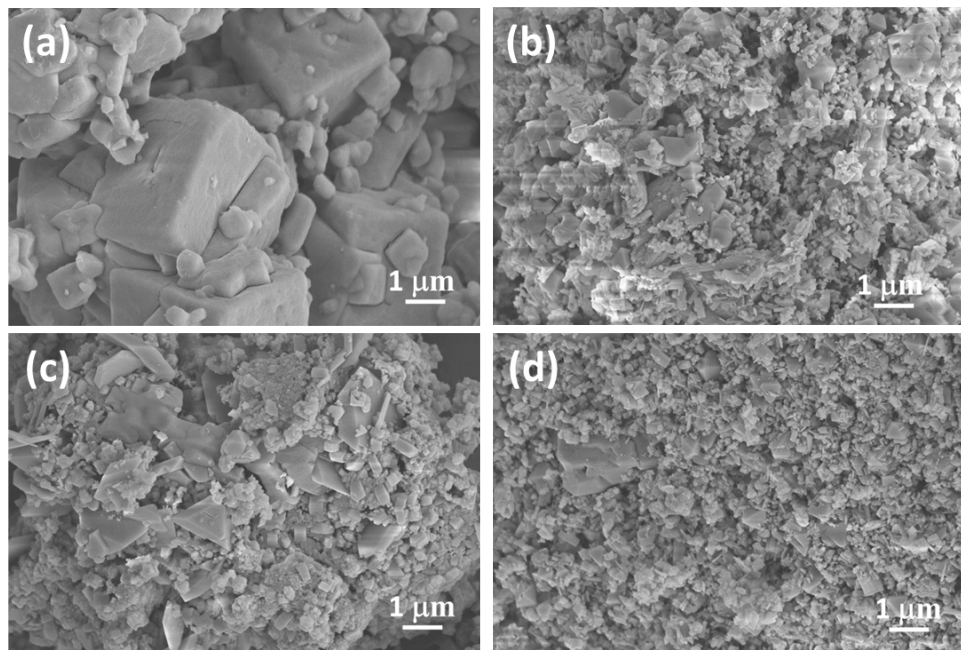


Figure S5: SEM images of (a) IF precursor, (b) pyrochlore-NH₄Fe₂F₆, (c) TTB-K_{0.58}FeF₃, and (d) weberite-Na₂Fe₂F₇.

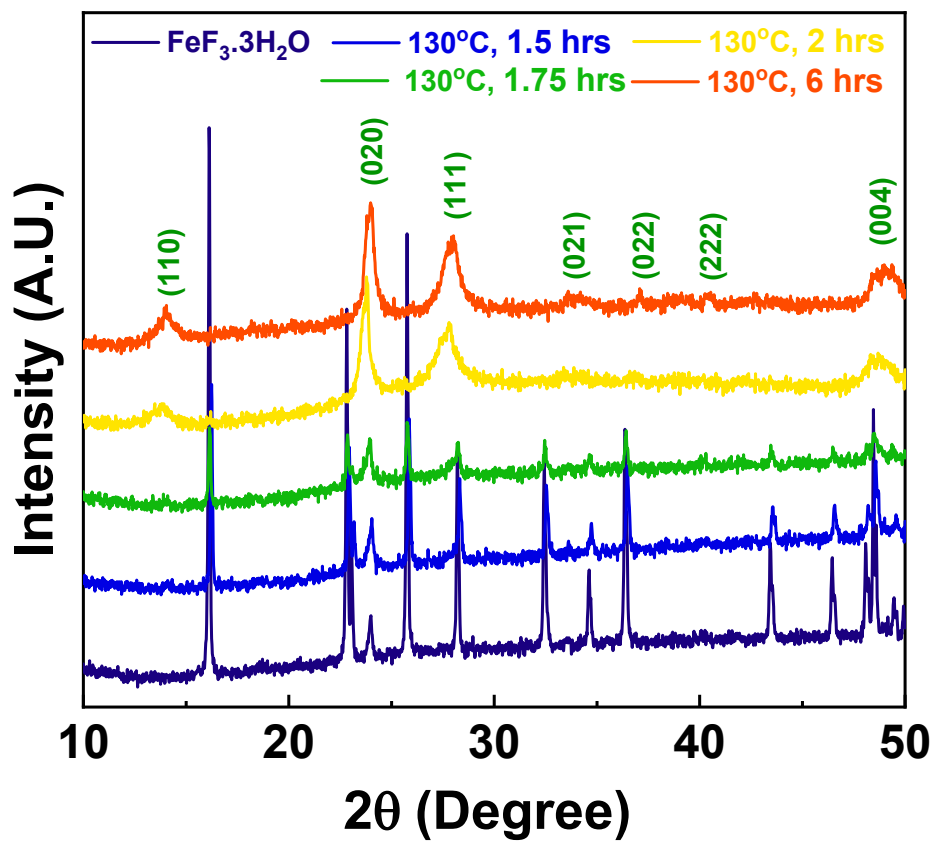


Figure S6: XRD patterns of products collected upon heating the IF precursor to 130°C for various time lengths.

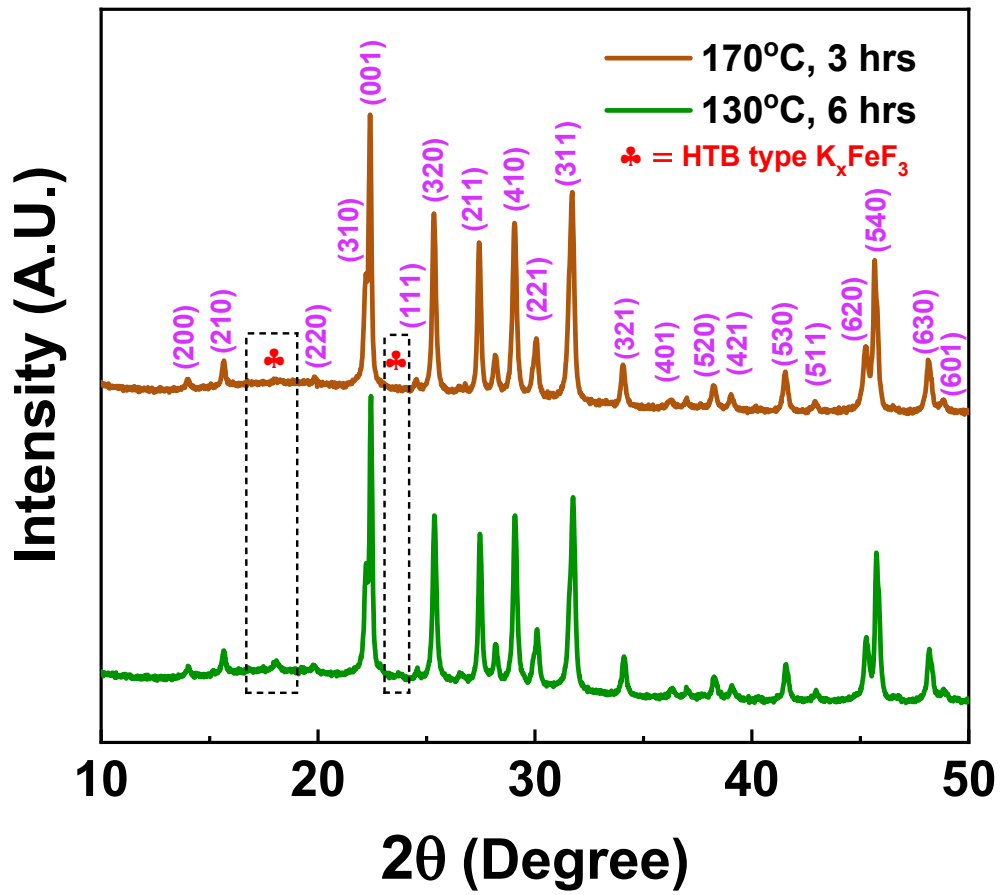


Figure S7: Comparison between XRD patterns of the products from the reactions of KI:IF = 1:1, at 130 and 170°C.

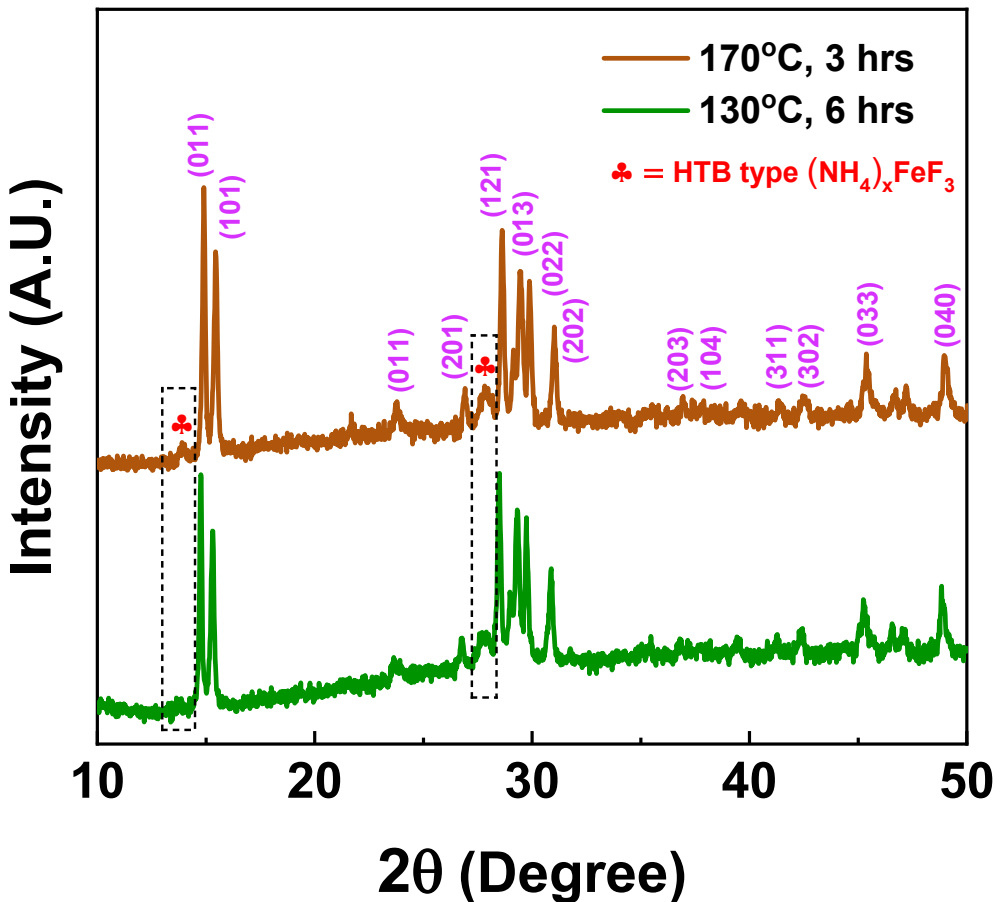


Figure S8: Comparison between XRD patterns of the products from the reactions of $\text{NH}_4\text{I:IF} = 1:1$ at 130°C and 170°C .

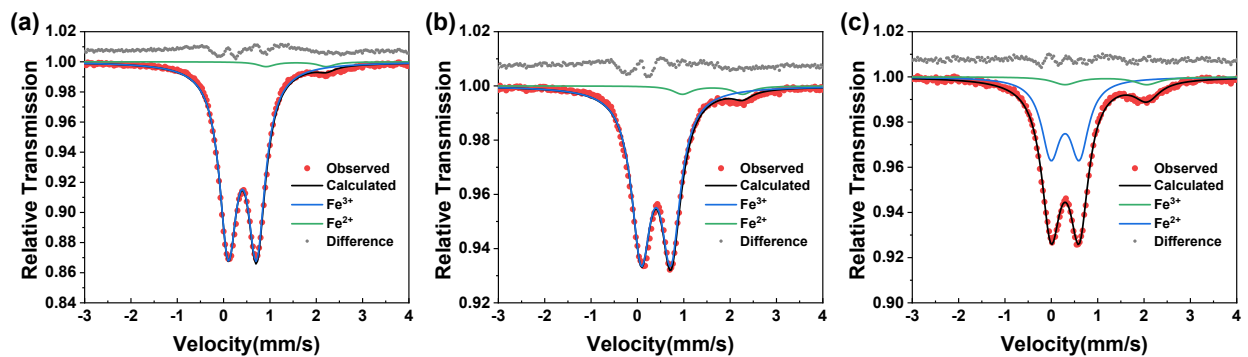


Figure S9: Mössbauer spectroscopy data of the products after reacting (a) NaI (b) KI and (c) NH_4I with IF in a 0.25:1.0 ratio.

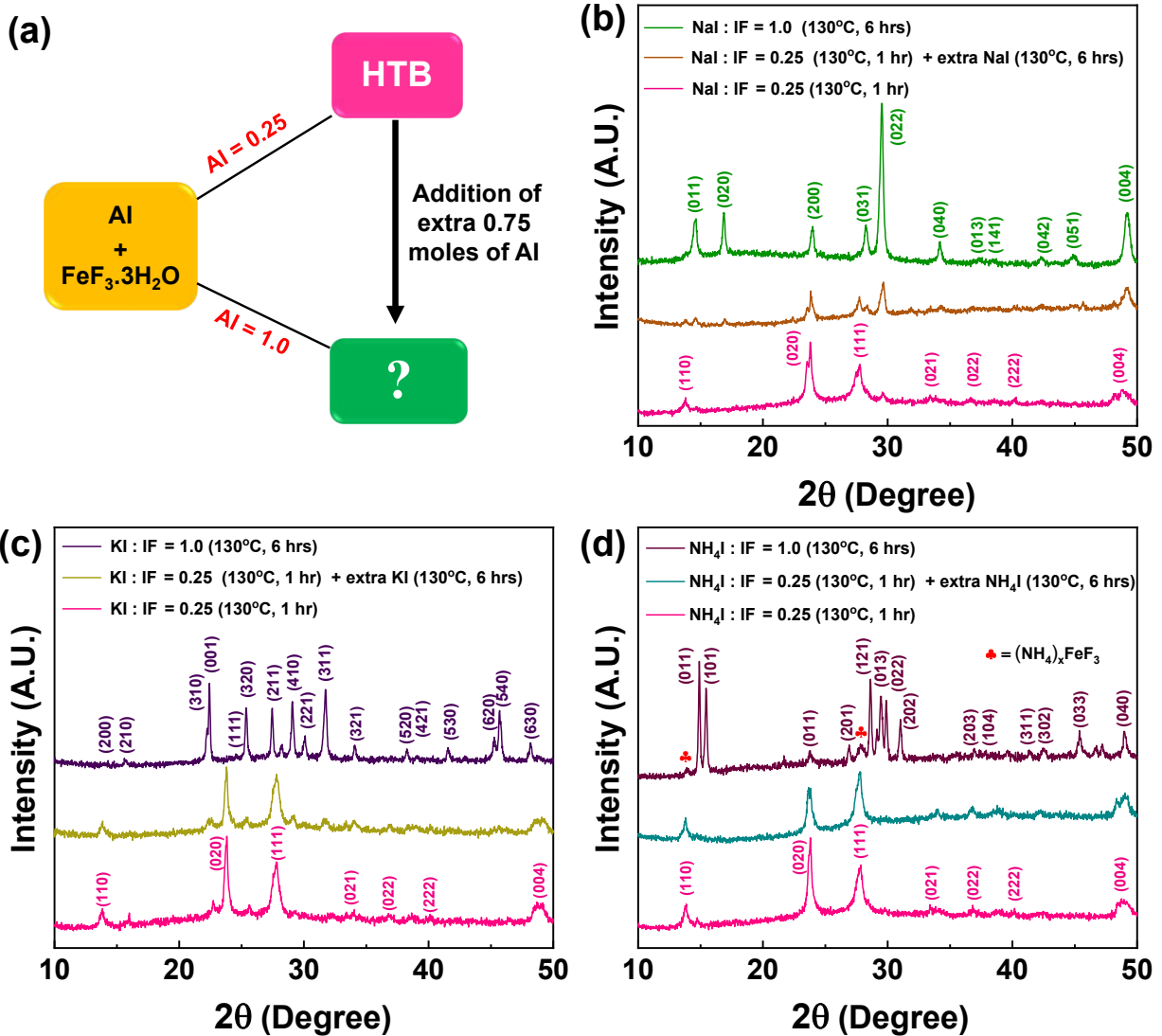


Figure S10: (a) Schematic representation to convert a low AI concentration product to a high AI concentration product via a two-step process. Comparison of XRD patterns of the products formed at low, high and (low + extra) concentration of (b) NaI, (c) KI, and (d) NH₄I.

Iron Fluoride Structures

In this work, we used a primitive cell for all frameworks considered, except where we considered a $2 \times 1 \times 1$ supercell for $K_{0.6}FeF_3$ (20 formula unit), since the primitive cell did not represent the correct magnetization for Fe. From previous experimental work, iron fluoride perovskites exist as orthorhombic ($NaFeF_3$)² or cubic ($KFeF_3$)³ phases. In order to get the correct ground state structure, we calculated the total ground state energy by inserting each cation (Na^+ , K^+ , NH_4^+) within both phases. As a result, we find that Na and NH_4 prefer the orthorhombic perovskite structure while K prefers the cubic structure.

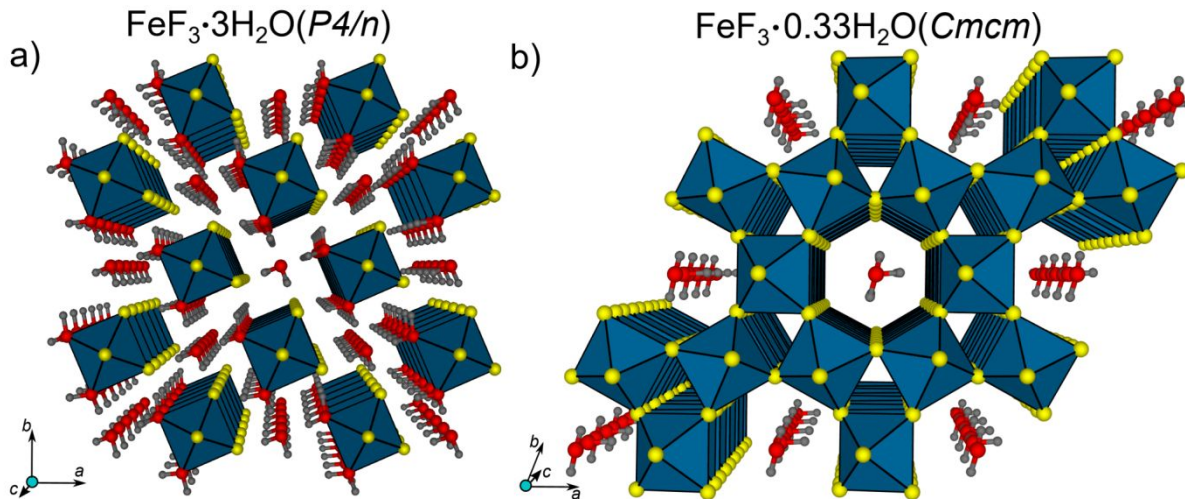


Figure S11: The crystal structure of (a) one-dimensional $FeF_3 \cdot 3H_2O$ (IF) and (b) a hexagonal tungsten bronze (HTB) type $FeF_3 \cdot 0.33H_2O$. The FeF_6 octahedron is indicated by a deep-sky-blue color polyhedra, where the yellow, red and grey spheres represent fluorine, oxygen and hydrogen atom, respectively.

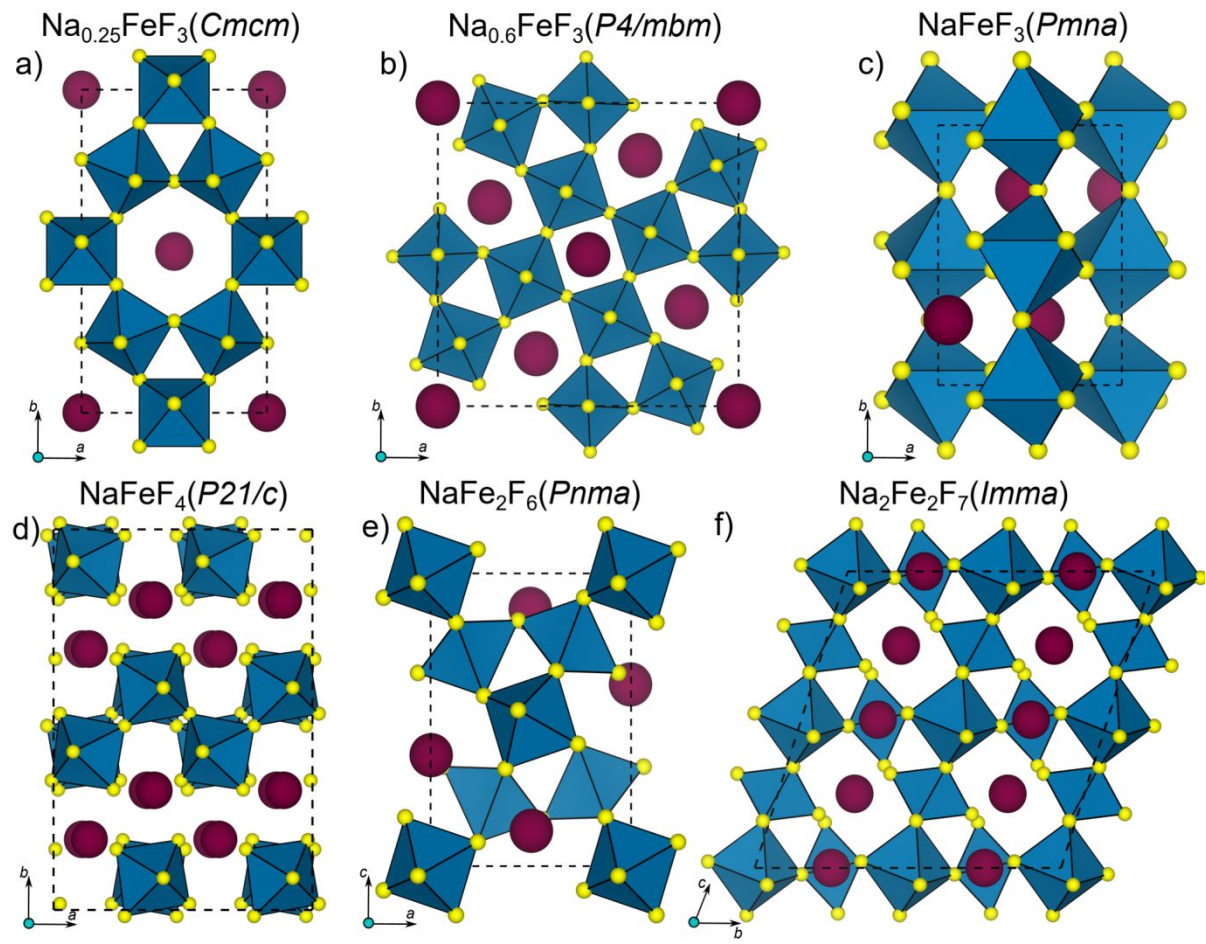


Figure S12: Representative crystal structure of (a) HTB- $\text{Na}_{0.25}\text{FeF}_3$, (b) tetragonal tungsten bronze (TTB)- $\text{Na}_{0.6}\text{FeF}_3$, (c) perovskite- NaFeF_3 , (d) NaFeF_4 , (e) pyrochlore- NaFe_2F_6 , (f) weberite- $\text{Na}_2\text{Fe}_2\text{F}_7$ frameworks. The maroon color sphere represents a Na atom. Notations in the figure are identical to **Figure S11**.

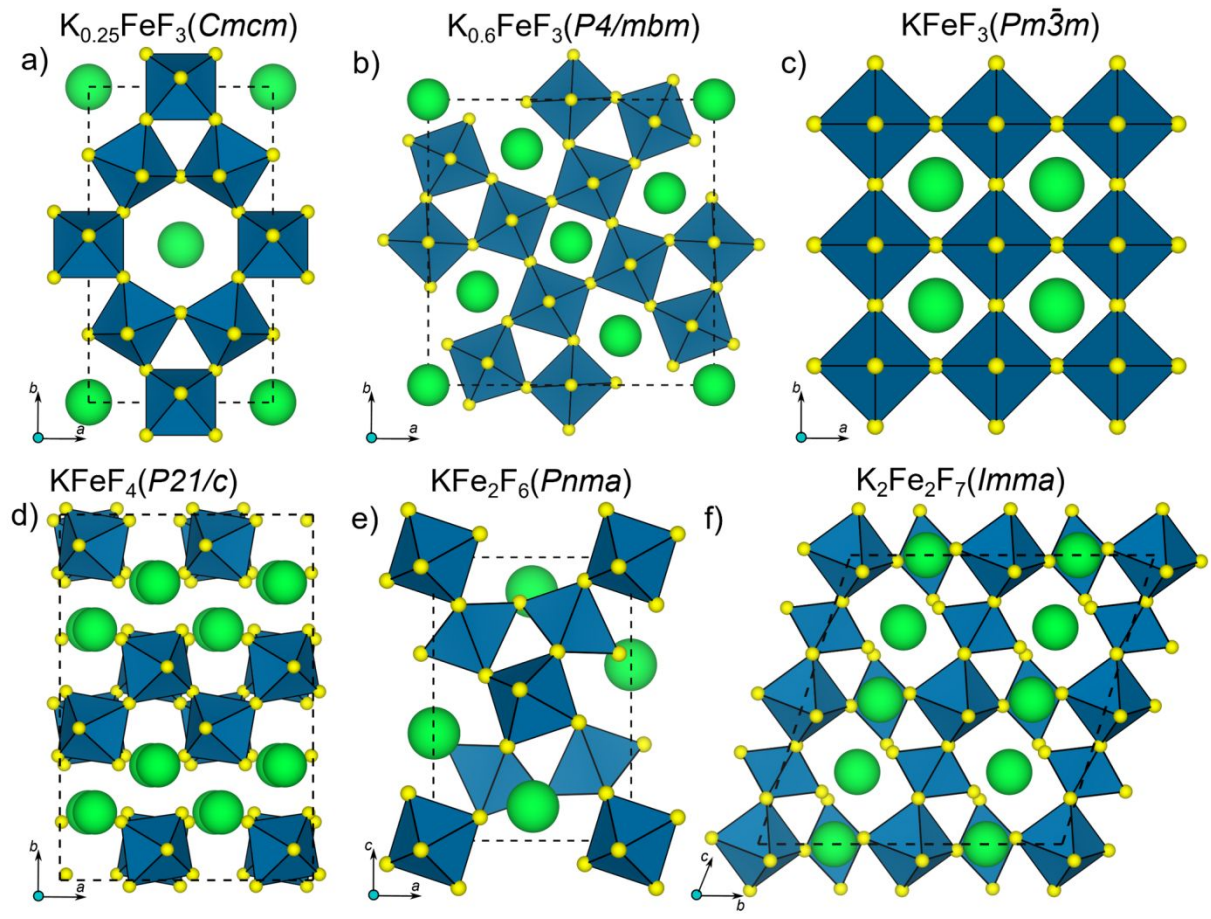


Figure S13: Representative crystal structure of (a) HTB- $\text{K}_{0.25}\text{FeF}_3$, (b) TTB- $\text{K}_{0.6}\text{FeF}_3$, (c) perovskite- KFeF_3 , (d) KFeF_4 , (e) pyrochlore- KFe_2F_6 , (f) weberite- $\text{K}_2\text{Fe}_2\text{F}_7$ frameworks. The green color sphere represents a K atom. Notations in the figure are identical to **Figure S11**.

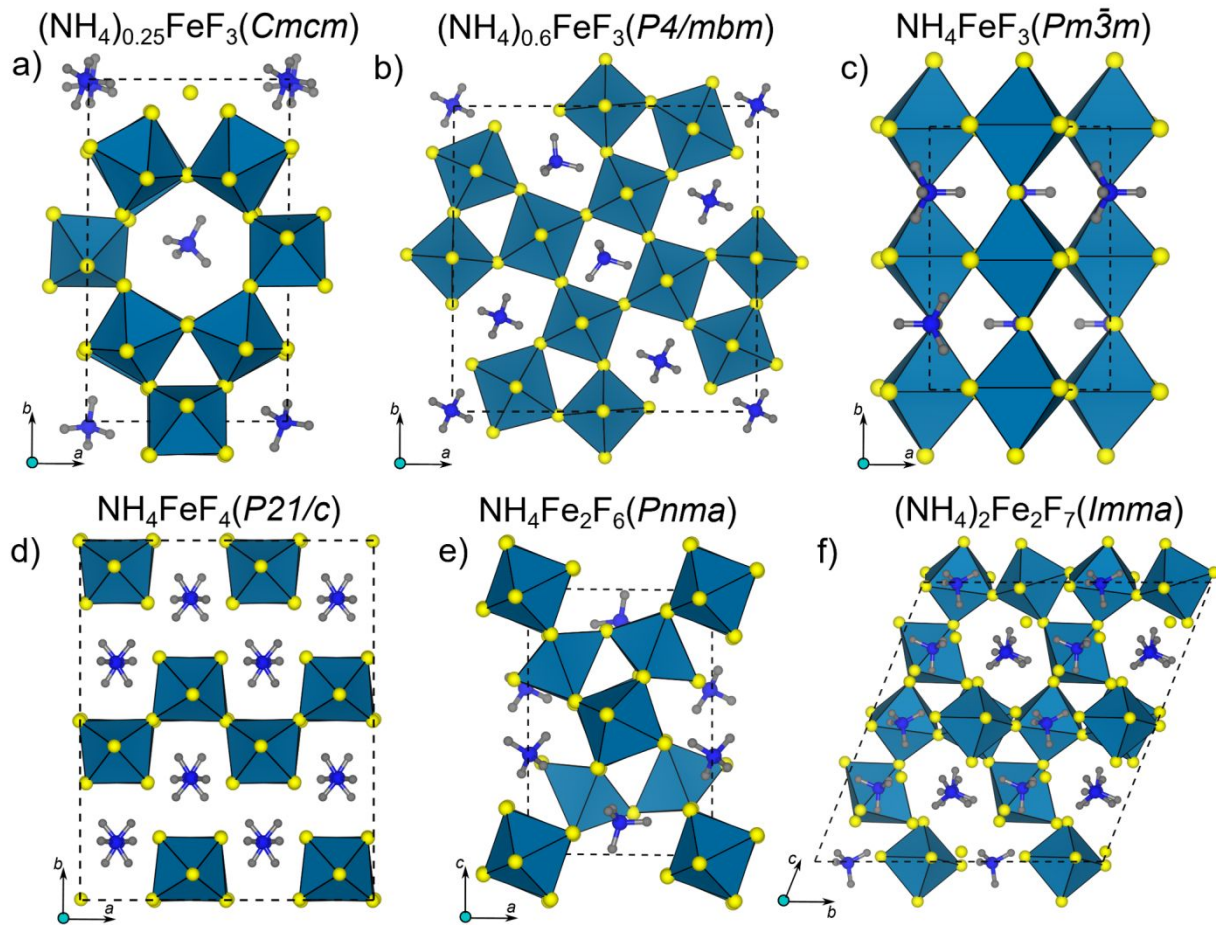


Figure S14: Representative crystal structure of (a) HTB- $(\text{NH}_4)_{0.25}\text{FeF}_3$, (b) TTB- $(\text{NH}_4)_{0.6}\text{FeF}_3$, (c) perovskite- NH_4FeF_3 , (d) NH_4FeF_4 , (e) pyrochlore- $\text{NH}_4\text{Fe}_2\text{F}_6$, (f) weberite- $(\text{NH}_4)_2\text{Fe}_2\text{F}_7$ frameworks. The blue color sphere represents element N. Notations in the figure are identical to **Figure S11**.

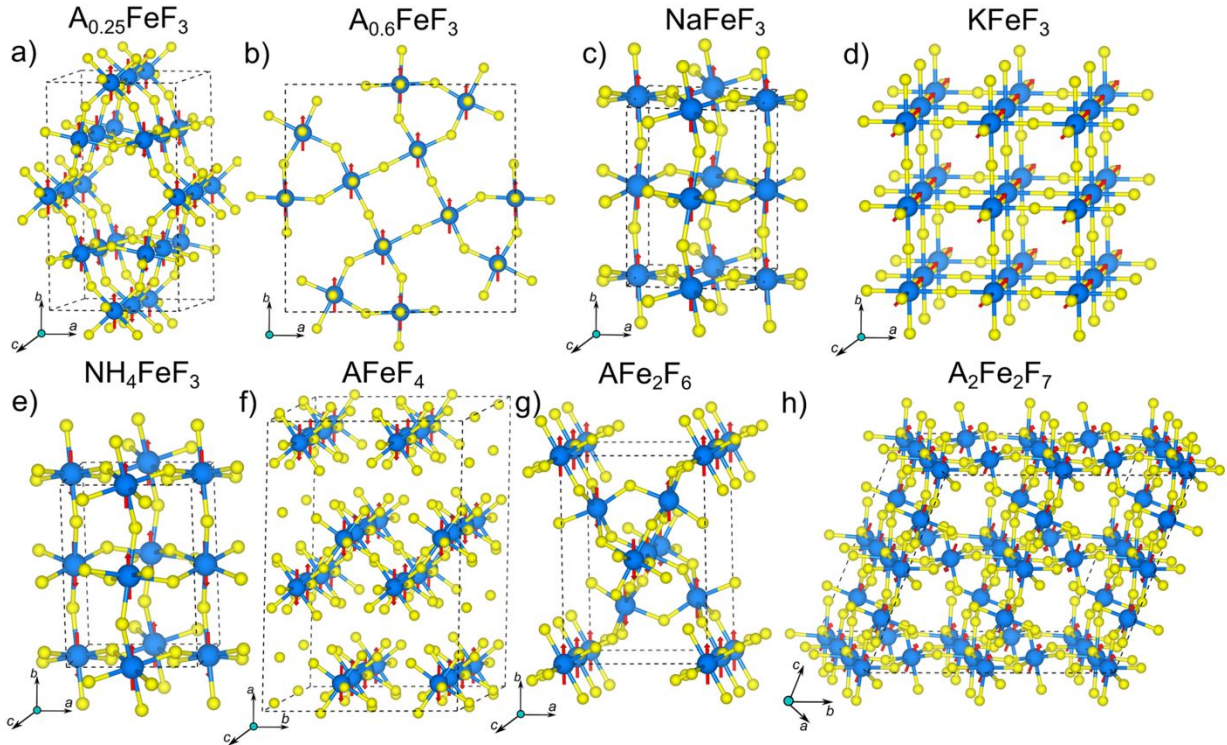


Figure S15: The magnetic configurations of Fe atoms in a representative iron fluoride frameworks, as calculated using DFT. The light blue and yellow spheres represent the Fe and F atoms, respectively, while A represents Na, K, or NH₄. The A atoms have been removed from all structures for clarity. The red arrow indicates the direction of the magnetic moment of the Fe atom. The magnetic moment of Fe atom is ordered antiferromagnetically in (a) HTB-A_{0.25}FeF₃, (e) perovskite-NH₄FeF₃, (f) AFeF₄, (g) pyrochlore-AFe₂F₆, (h) weberite-A₂Fe₂F₇ frameworks, while it is ordered ferromagnetically in (b) TTB-A_{0.6}FeF₃, (c) perovskite-NaFeF₃², and (d) perovskite-KFeF₃⁴ frameworks. Across all iron fluoride frameworks, the magnetic moment ordering of Fe is identical regardless of the A cations, except in the perovskite framework, where NaFeF₃ and KFeF₃ exhibit a ferromagnetic ordering, while NH₄FeF₃ displays an antiferromagnetic ordering. In cases where magnetic ordering information for the frameworks was not available in the literature, we determined the ground state magnetic ordering through density functional theory (DFT) calculations, considering both ferromagnetic and antiferromagnetic ordering.

Hubbard U correction for Fe in iron fluorides

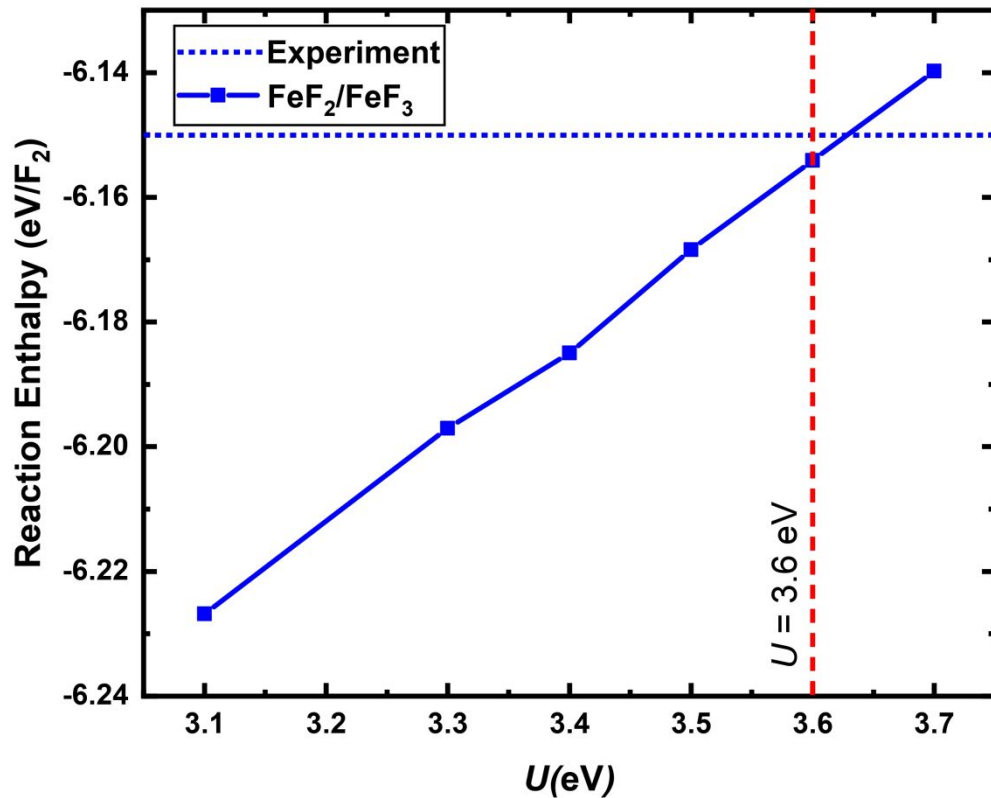


Figure S16: Oxidation (fluorination) reaction enthalpy (blue solid line) variation with increasing U within the SCAN+ U frameworks for Fe in iron fluorides. The Horizontal dotted line represents the experimental reaction enthalpy of $\text{FeF}_2/\text{FeF}_3$. The vertical dashed red line indicates a Hubbard U correction of 3.6 eV for Fe, which minimizes the error between the DFT calculated and experimental reaction enthalpy.

0 K Phase Diagrams of Na-Fe-F, K-Fe-F and NH₄-Fe-F

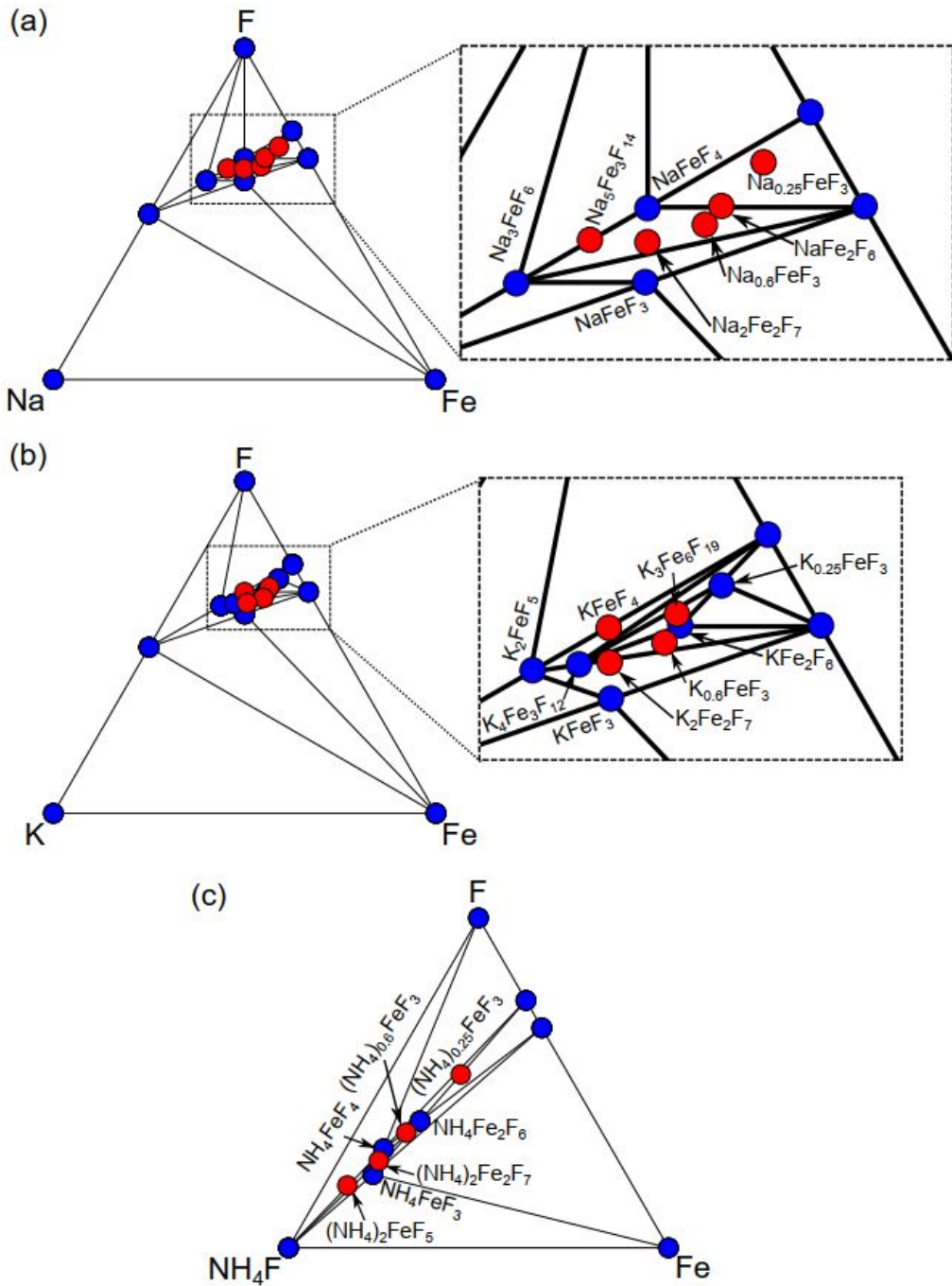


Figure S17: Calculated 0 K ternary phase diagram (convex hull) of (a) Na-Fe-F, (b) K-Fe-F and (c) NH₄-Fe-F. The solid blue circle represents stable compositions laying on/below the convex hull, whereas the solid red circle represents a metastable/unstable phase that lies above the convex hull. The black line denotes a tie line connecting a stable phase.

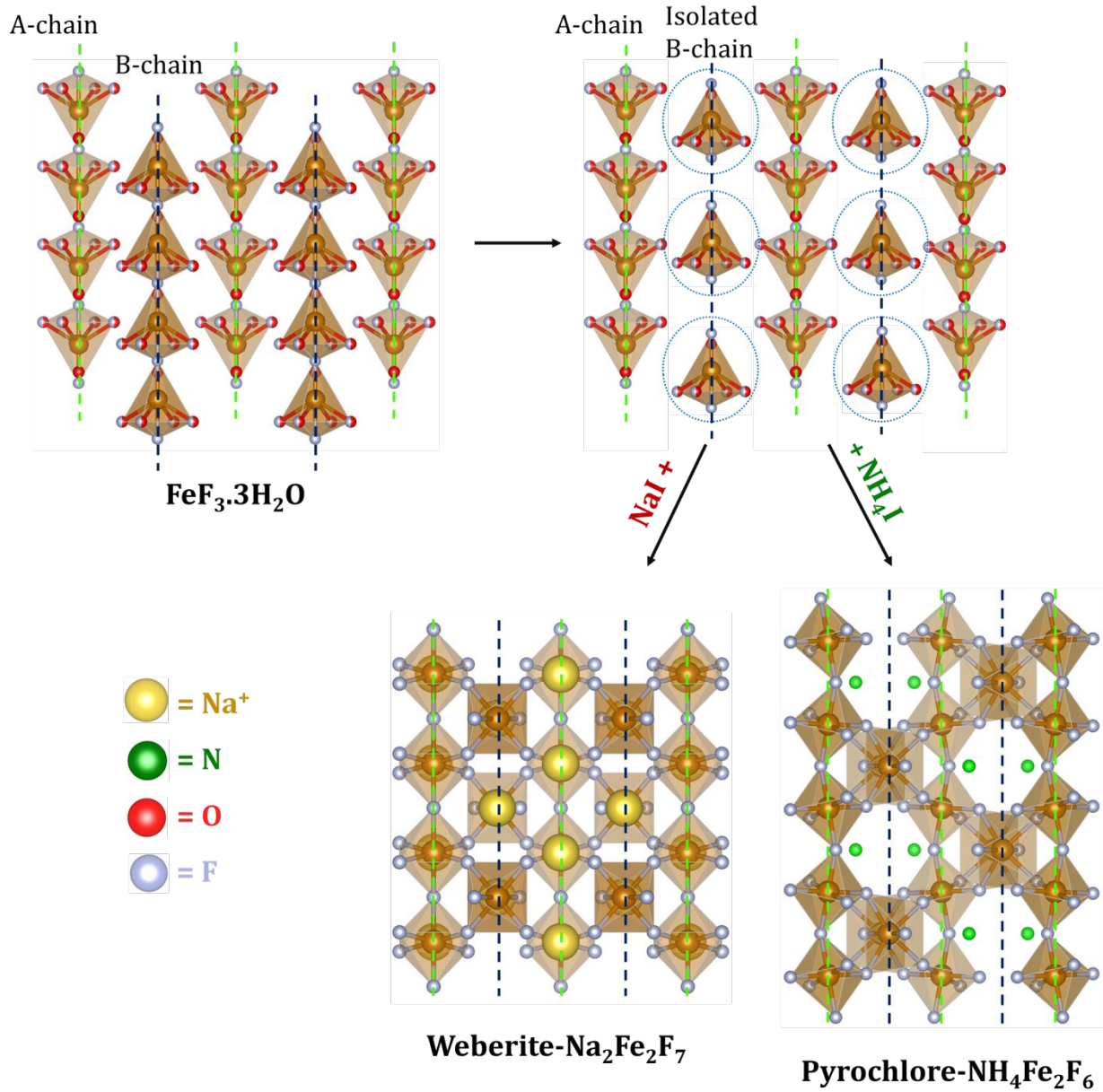


Figure S18: Schematic illustration of the topochemical transformation from 1D- $\text{FeF}_3 \cdot 3\text{H}_2\text{O}$ to 3D-weberite- $\text{Na}_2\text{Fe}_2\text{F}_7$ and pyrochlore- $\text{NH}_4\text{Fe}_2\text{F}_6$. During the transformation, half of the 1D chains (denoted as A-chain) are retained, while the other half of 1D chains (denoted as B-chain) break to form isolated FeF_6 units, which are then connected to A-chain through corner-sharing. The striking difference between the structures is that the isolated FeF_6 units in the weberite phase share four of their corners with 1D chains (A-chains) while the other two are connected with sodium polyhedra. On the contrary, all the corners of isolated FeF_6 units (from the B-chain) are shared with other FeF_6 (in both A and B-chains) units in the pyrochlore structure

Table S1: Structural parameters of Na₂Fe₂F₇ material.

Formula	Na ₂ Fe ₂ F ₇
Formula Weight	290.66
Temperature (K)	297
Wavelength (Å)	1.54056 & 1.54439
	Kα ₁ / Kα ₂ = 2
Crystal Symmetry	Orthorhombic
Space group	<i>Imma</i>
Lattice parameters:	
<i>a</i> (Å)	7.384 (2)
<i>b</i> (Å)	10.503(4)
<i>c</i> (Å)	7.411(5)
<i>V</i> (Å ³)	574.83(7)
α	90.00°
β	90.00°
γ	90.00°
Density (calc.) (gcm ⁻³)	3.392
2θ range for data collection (deg)	10-90
Refinement method	full-matrix least-squares on F ²
R indices	chi square= 2.08 Rp= 15.5 Rwp= 8.29
Atomic parameters:	

Atom	x	y	z	Occ.	U	Site	Sym.
1 Na	0.000	0.000	0.000	1.000	0.022(2)	4a	2/m..
2 Na	0.250	0.250	0.750	1.000	0.044(3)	4d	.2/m.
3 Fe	0.250	0.250	0.250	1.000	0.063(2)	4c	.2/m.
4 Fe	0.000	0.000	0.500	1.000	0.045(2)	4b	2/m..
5 F	0.000	0.250	0.133(1)	1.000	0.474(4)	4e	mm2
6 F	0.000	0.426(4)	0.726(4)	1.000	0.025(5)	8h	m..
7 F	0.212(5)	0.400(8)	0.440(0)	1.000	0.116(9)	16j1	

Table S2: Structural parameters of $\text{K}_{0.6}\text{FeF}_3$ material.

Formula	$\text{K}_{0.6}\text{FeF}_3$
Formula Weight	139.299
Temperature (K)	297
Wavelength (\AA)	1.54056 & 1.54439
	$\text{K}\alpha_1/\text{K}\alpha_2 = 2$
Crystal Symmetry	Tetragonal
Space group	$P4/mbm$
Lattice parameters:	
a (\AA)	12.663(6)
b (\AA)	12.661(8)
c (\AA)	7.929(5)
V (\AA^3)	1272.61(3)
α	90.00°
β	90.00°
γ	90.00°
Density (calc.) (gcm^{-3})	3.561
2θ range for data collection (deg)	10-90
Refinement method	full-matrix least-squares on F^2
R indices	chi square= 1.90 R_p = 13.6 R_{wp} = 8.74

Atomic parameters:

Atom	<i>x</i>	<i>y</i>	<i>z</i>	Occ.	<i>U</i>	Site	Sym.
1 K	0.172(9)	0.326(0)	0.000	1.000	0.042(4)	4g	m.2 m
2 K	0.000	0.000	0.000	1.000	0.020(2)	2a	4/m..
3 Fe	0.500	0.000	0.500	1.000	0.010(1)	2c	m.m m
4 Fe	0.212(1)	0.075	0.500	1.000	0.010(1)	8j	m..
5 F	0.142(5)	-0.068(0)	0.500	1.000	0.030(9)	8j	m..
6 F	0.280(3)	0.219(6)	0.500	1.000	0.025(5)	4h	m.2 m
7 F	0.340(1)	-0.007(7)	0.500	1.000	0.044(4)	8j	m..
8 F	0.500	0.000	0.000	1.000	0.085(2)	2d	m.m m
9 F	0.206(0)	0.077(1)	0.000	1.000	0.030(5)	8i	m..

Table S3: Structural parameters of NH₄Fe₂F₆ material.

Formula	NH ₄ Fe ₂ F ₆
Formula Weight	243.72
Temperature (K)	297
Wavelength (Å)	1.54056 & 1.54439 Kα ₁ / Kα ₂ = 2
Crystal Symmetry	Orthorhombic
Space group	<i>Pnma</i>
Lattice parameters:	
<i>a</i> (Å)	7.058(1)
<i>b</i> (Å)	7.454(0)
<i>c</i> (Å)	10.146(0)
<i>V</i> (Å ³)	533.80(2)
α	90.00°
β	90.00°
γ	90.00°
Density (calc.) (gcm ⁻³)	2.818
2θ range for data collection (deg)	10-90
Refinement method	full-matrix least-squares on F ²
R indices	chi square= 2.71 Rp= 19.3 Rwp= 11.4

Atomic parameters:

Atom		<i>x</i>	<i>y</i>	<i>z</i>	Occ.	<i>U</i>	Site	Sym.
1 N		-0.029(0)	0.250	0.757(2)	1.000	0.008(8)	4c	.m.
2 Fe		0.000	0.000	0.000	1.000	0.001(1)	4a	-1
3 Fe		0.238(3)	0.250	0.234(8)	1.000	0.001(1)	4c	.m.
4 F		-0.155(6)	0.250	0.220(1)	1.000	0.002(2)	4c	.m.
5 F		0.004(7)	0.250	0.943(1)	1.000	0.002(2)	4c	.m.
6 F		0.203(3)	0.408(1)	0.147(5)	1.000	0.010(5)	8d	1
7 F		0.737(5)	0.431(8)	0.098(2)	1.000	0.226(8)	8d	1

Table S4: Parameters of the fitted Mössbauer spectroscopy data.

Sample	Γ (mm/s)	IS (mm/s)	QS (mm/s)	% Area
Weberite- $\text{Na}_{1.99}\text{Fe}_2\text{F}_7$	0.45 ± 0.01	0.29 ± 0.01	0.67 ± 0.01	70 (Fe ³⁺)
	0.63 ± 0.02	1.16 ± 0.01	1.63 ± 0.01	30 (Fe ²⁺)
TTB- $\text{K}_{0.58}\text{FeF}_3$	0.43 ± 0.01	0.44 ± 0.01	0.51 ± 0.01	47 (Fe ³⁺)
	0.69 ± 0.02	1.36 ± 0.03	1.86 ± 0.02	53 (Fe ²⁺)
Pyrochlore- $\text{NH}_4\text{Fe}_2\text{F}_6$	0.43 ± 0.01	0.44 ± 0.01	0.67 ± 0.01	68 (Fe ³⁺)
	0.35 ± 0.02	1.32 ± 0.03	2.67 ± 0.02	32 (Fe ²⁺)
HTB- Na_xFeF_3	0.46 ± 0.02	0.40 ± 0.01	0.61 ± 0.01	97 (Fe ³⁺)
	0.46 ± 0.02	1.45 ± 0.04	1.30	3 (Fe ²⁺)
HTB- K_xFeF_3	0.50 ± 0.02	0.40 ± 0.01	0.64 ± 0.01	95 (Fe ³⁺)
	0.50 ± 0.02	1.45 ± 0.04	1.30	5 (Fe ²⁺)
HTB-(NH_4) _x FeF_3	0.49 ± 0.01	0.30 ± 0.01	0.61 ± 0.01	84 (Fe ³⁺)
	0.65 ± 0.02	1.18 ± 0.01	1.77 ± 0.01	16 (Fe ²⁺)

Table S5: Summary of ¹H NMR fitting parameters.

	Chemical Shift (δ)	Full Width Half Max (FWHM)	Integrated Intensity	Gaussian (100%) vs. Lorentzian (0%) Peak shape
$\text{FeF}_3 \bullet 3\text{H}_2\text{O}$	188	109	44%	0%
	-9	42	56%	1%
$\text{FeF}_3 \bullet 0.33\text{H}_2\text{O}$	187	93	27%	100%
	2	15	34%	0%
$(\text{NH}_4)_{0.18}\text{FeF}_3$	60	54	40%	68%
	187	91	13%	100%
$\text{NH}_4\text{Fe}_2\text{F}_6$	2	15	21%	0%
	47	48	31%	0%
	19	37	36%	100%
	76	33	70%	50%
	7	41	21%	100%
	47	31	8%	100%

Table S6: The predicted adjacent phases for all stable iron fluorides (A -Fe-F, $A = \text{Na}^+$, K^+ , or NH_4^+) and their E^{Hull} values obtained from convex hull calculations are presented. Note that for all stable entities on a phase diagram, energy below the convex hull represents the formation energy of the stable phase with respect to the adjacent stable phases on the convex hull.

No.	Iron Fluoride Frameworks	Adjacent phases	E^{Hull} (meV/atom)
Na-Fe-F			
1	NaFeF_4	Na_3FeF_6 , FeF_3	-5
2	NaFeF_3	FeF_2 , NaF	-11
K-Fe-F			
3	KFe_2F_6	$\text{K}_4\text{Fe}_3\text{F}_{12}$, $\text{K}_{0.25}\text{FeF}_3$, FeF_2	-1
4	KFeF_3	FeF_2 , KF	-92
NH₄-Fe-F			
5	$\text{NH}_4\text{Fe}_2\text{F}_6$	FeF_3 , NH_4FeF_3	-26
6	NH_4FeF_4	FeF_3 , NH_4F	-13
7	NH_4FeF_3	NH_4F , FeF_2	-25

Table S7: The predicted decomposition products for all unstable or metastable iron fluoride frameworks and their E^{Hull} values obtained from convex hull calculations are presented.

No.	Iron Fluoride Frameworks	Decomposition products	E^{Hull} (meV/atom)
Na-Fe-F			
1	NaFe_2F_6	NaFeF_4 , FeF_2	83
2	$\text{Na}_2\text{Fe}_2\text{F}_7$	NaFeF_4 , Na_3FeF_6 , FeF_2	16
3	$\text{Na}_{0.6}\text{FeF}_3$	NaFeF_4 , Na_3FeF_6 , FeF_2	52
4	$\text{Na}_{0.25}\text{FeF}_3$	NaFeF_4 , FeF_2 , FeF_3	32
K-Fe-F			
5	KFeF_4	K_2FeF_5 , FeF_3	8
6	$\text{K}_2\text{Fe}_2\text{F}_7$	$\text{K}_4\text{Fe}_3\text{F}_{12}$, FeF_2	15

7	$K_{0.6}FeF_3$	KFe_2F_6 , $K_4Fe_3F_{12}$, FeF_2	1
8	$K_{0.25}FeF_3$	KFe_2F_6 , FeF_3	1
NH₄-Fe-F			
9	$(NH_4)_2Fe_2F_7$	$NH_4Fe_2F_6$, NH_4F	1
10	$(NH_4)_{0.6}FeF_3$	$NH_4Fe_2F_6$, NH_4FeF_3	14
11	$(NH_4)_{0.25}FeF_3$	$NH_4Fe_2F_6$, FeF_3	18

References:

- (1) Hung, I.; Zhou, L.; Pourpoint, F.; Grey, C. P.; Gan, Z. Isotropic High Field NMR Spectra of Li-Ion Battery Materials with Anisotropy >1 MHz. *J. Am. Chem. Soc.* **2012**, *134* (4), 1898–1901. <https://doi.org/10.1021/ja209600m>.
- (2) Bernal, F. L. M.; Gonano, B.; Lundvall, F.; Wragg, D. S.; Fjellv+Ng, H.; Veillon, F.; Séawiäski, W. A.; Fjellvng, Ÿ. S. Canted Antiferromagnetism in High-Purity NaFeF₃ Prepared by a Novel Wet-Chemical Synthesis Method. *Phys. Rev. Mater.* **2020**, *4* (11), 1–8. <https://doi.org/10.1103/PhysRevMaterials.4.114412>.
- (3) Knox, K. Perovskite-like Fluorides. I. Structures of KMnF₃, KFeF₃, KNiF₃ and KZnF₃. Crystal Field Effects in the Series and in KCrF₃ and KCuF₃. *Acta Crystallogr.* **1961**, *14* (6), 583–585. <https://doi.org/10.1107/s0365110x61001868>.
- (4) Ito, A.; Morimoto, S. Mössbauer Study of Magnetic Properties of KFeF₃. *J. Phys. Soc. Japan* **1975**, *39* (4), 884–891. <https://doi.org/10.1143/JPSJ.39.884>.